Structural characterization of nanoparticles-assembled titanium dioxide films produced by ultrafast laser ablation and deposition in background oxygen

S. Amoruso [a,b,*], S. Tuzi [a], D.K. Pallotti [a], C. Aruta [b], R. Bruzzese [a,b], F. Chiarella [c], R. Fittipaldi [c], S. Lettieri [b], P. Maddalena [a,b], A. Sambri [a], A. Vecchione [c], X. Wang [b]

[a] *Dipartimento di Fisica, Complesso Universitario di Monte Sant'Angelo, Via Cintia, I-80125 Napoli, Italy*
[b] *CNR-SPIN UOS Napoli, Complesso Universitario di Monte Sant'Angelo, Via Cintia, I-80125 Napoli, Italy*
[c] *CNR-SPIN UOS Salerno, via Ponte don Melillo, I -84084 Fisciano (SA), Italy*

ARTICLE INFO

ABSTRACT

Ultrafast laser ablation of titanium dioxide and deposition of nanoparticles-assembled films in oxygen ambient gas at pressures going from high-vacuum up to several mbar is investigated. We identify various regimes of the plumes propagation into the background gas as well as of the material deposition rate. These reflect on the structural characteristics of the nanoparticles-assembled films: the film morphology changes from a structure with glue-like nanoparticulates, at low pressure, to a highly porous assembly of individual nanoparticles, at larger pressure. Our findings indicate that background gas pressure provides an interesting key for additional control on the structural characteristics of oxide nanostructures produced by femtosecond laser deposition.

© 2013 Elsevier B.V. All rights reserved.

1. Introduction

Ultrafast laser ablation (ULA) is the explosive removal of material excited to high temperature and pressure through irradiation with intense laser pulses of femtosecond (fs) duration. ULA in high vacuum has been rather extensively investigated, evidencing that it leads to the direct generation of nanoparticles (NPs) of the target material [1–4]. Deposition of the ULA material on a suitable substrate offers a practical route for the synthesis of NPs and NPs-assembled films of different materials by pulsed laser deposition (PLD) [3–7]. PLD with femtosecond pulses (fs-PLD) has been applied for the growth of oxide thin films [8,9], as well as of oxide nanostructures in the form of nanoparticles, nanorods and nanowires assembly [10–12]. For example, catalyst-free growth of oxides nanorods was achieved by fs-PLD in a low pressure background gas (N_2 and O_2 mixture at $\approx 10^{-2}$ mbar) [11]. Moreover, oxide nanowires were obtained at atmospheric pressure by fs-PLD assisted by Au NPs acting as catalyst on the substrate surface [12].

The use of an ambient gas is a well-established method employed in the PLD technique to control highly energetic species since the gas acts as a moderator of the ablation plume during the flight from the target to the substrate [13,14]. The study of the interaction of ablation plumes with a background gas has been considered rather extensively for nanosecond pulses [13–17], while studies aiming to ascertain meaningful correlations among the different ULA parameters, the structural and functional properties of the deposited films, and the plume dynamics in a background gas are still scarce [18–20].

In this letter, we examine the effects of the ambient gas pressure (from high-vacuum up to ≈ 10 mbar) during fs-PLD of titanium dioxides (TiO_2), a wide bandgap (3.0–3.2 eV) semiconductor which in nanostructured form is considered as a very relevant material for a number of emerging applications, crossing traditional disciplinary boundaries in energy and environmental technologies [21–24]. TiO_2 has excellent optical and electronic properties for a widespread use (e.g., in photocatalytic air purification and environmental sanitation, self-cleaning coatings and electrodes for photovoltaic solar energy conversion, gas sensing, etc.). As for other functional oxides, e.g., tin oxide and zinc oxide [25–27], the nanostructure characteristics critically influence the performances of TiO_2-based devices, particularly those based on photocatalysis, and

* Corresponding author at: Dipartimento di Fisica, Complesso Universitario di Monte Sant'Angelo, Via Cintia, I-80125 Napoli, Italy. Tel.: +39 081 679 287.
E-mail addresses: amoruso@na.infn.it, salvatore.amoruso@unina.it (S. Amoruso).

reactivity to changes in the external environment [28]. Developing well-controlled routes for the synthesis of high-quality TiO_2 nanostructures can thus be of relevance to many applications.

Several studies have been carried out on the fabrication of TiO_2 nanostructured films by PLD with nanosecond laser pulses (see, e.g., Refs. [29]–[31], and papers therein quoted). These studied evidence the production of TiO_2 nanostructured, crystalline deposits whose properties depend on the deposition conditions, namely background gas (vacuum, Ar and O_2) pressure and laser pulse wavelength. In some cases a pure Ti target is ablated and titanium dioxide is formed either in the interaction with oxygen background gas or on the substrate [32]. Optical emission spectroscopy analysis of the TiO_2 ablation plume showed the presence of Ti and O neutrals and Ti ions, while no sizeable signature of emission from excited molecules or nanoclusters was observed in the registered spectra. Nevertheless, microscopic particles were present on the surface deposits, which reduce at shorter wavelength (e.g., 266 nm). On the contrary, the few previous studies on fs-PLD of TiO_2, carried out in high vacuum or at low oxygen background pressure ($\approx 10^{-2}$ mbar), have shown that nearly stoichiometric TiO_2 NPs with average diameters of ≈ 20–50 nm are produced [10,32]. Moreover, ablation plume analyses in high vacuum conditions show the presence of a significant component of NPs in the ablated material, and the nanostructured deposit mainly results from the collection of these NPs on the substrate [10,32].

Here we investigate the influence of the background oxygen pressure on the properties of TiO_2 NPs-assembled films, from high vacuum up to several mbar. Our experimental findings demonstrate an interesting influence of the background gas pressure: the film morphology changes from a cauliflower-like structure with NPs embedded in glue-like nanoagglomerates, at low pressure, to a highly porous assembly of individual NPs, at larger pressure. This observation is correlated with the NPs plume dynamics and deposition rate dependence on the background gas pressure. These outcomes are particularly relevant to tune oxide NPs films characteristics for applications where the nanoscale porosity, and the high-surface brought about by the NPs can be beneficial to facilitate reactions with the interacting medium as, e.g., in photocatalytic and sensing applications.

2. Experimental methods

Fs laser pulses (527 nm, ≈ 300 fs full width at half maximum) were used to produce ablation of a commercial TiO_2 rutile target (SurfaceNet). The laser beam was focused at $\approx 45°$ onto the target surface with a 25 cm focal length lens. By measurement of the laser impact region as a function of the laser pulse energy [33,34], a spot area on the target of $(4.4 \pm 0.4) \times 10^{-4}$ cm^2 was estimated. Ablation was induced by laser pulses at a fluence of 1.4 J/cm^2, corresponding to about $10\times$ the TiO_2 damage threshold for 527 nm, ≈ 300 fs laser pulses [35]. The target was mounted on a rotating holder to avoid local drilling.

NPs-assembled films were deposited by collecting the produced NPs on Si(1 0 0) substrates, held at room temperature and located 4.0 cm a part from the target surface. The morphology of the TiO_2 NPs-assembled films was analyzed by a Zeiss ΣIGMA field emission scanning electron microscope (FESEM) with a nominal resolution of 1.3 nm at 20 kV, while their crystallographic structure was investigated by means of X-ray diffraction (XRD), using a Rigaku D/Max-B powder diffractometer with Cu Kα radiation, in the θ/2θ configuration. The diagnostic tools for the analysis of the fs-PLD process included a fast intensified-charge-coupled device (ICCD) for time- and space-resolved imaging of the ULA plumes, and a quartz crystal microbalance (QCM). The deposition rate measurements were carried out by placing the QCM at the substrate location.
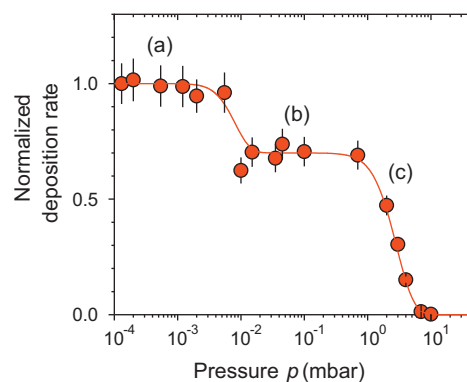
Fig. 1. Variation of the deposition rate as a function of the background oxygen pressure, p. The deposition rate is normalized to the value registered in high vacuum. The solid curve is a guide to the eye. The letters identify the three different regimes characterizing the pressure dependence of the deposition rate.

Typically, ≈ 3300 laser pulses at 33 Hz were used for deposition rate measurements, due to the QCM limited sensitivity. Plume images were acquired by reducing the rep. rate at ≈ 1 Hz with a mechanical shutter and accumulating 10 laser ablation events.

3. Results and discussion

Fig. 1 reports the relative variation of the deposition rate as a function of the background gas pressure, p. In Fig. 1, the deposition rate is normalized to the value (12 ± 1 ng/s) registered in high vacuum (HV). We can clearly identify the existence of three different deposition regimes. At low pressure, a constant deposition rate is observed for $p < 2 \times 10^{-3}$ mbar [regime (a)]. At intermediate pressure ($10^{-2} < p < 10^{-1}$; mbar), this is followed by a plateau region characterized by a $\approx 30\%$ reduction of the deposition rate with respect to HV [regime (b)]. Then, for $p > 1$ mbar, a third region, characterized by a progressive decrease of the deposition rate [regime (c)], is observed. This behavior can be related to the effects of the background gas pressure on ULA plume species [18]. In fact, the ablated material produced during ULA of TiO_2 consists of two main components [35], similarly to what is generally observed in ULA of metals and elemental semiconductors [1,2,4]. An atomic/molecular plume, composed of Ti and TiO species, and flowing at high velocity ($\approx 10^4$ m/s), is followed by a slower population of aggregates (clusters and NPs), which expands at a much smaller velocity ($\approx 5 \times 10^2$ m/s) [35]. The oxygen background gas, acting differently on the atomic and NPs plumes [18], gives rise to the presence of the different regimes observed in Fig. 1.

Fig. 2(a) reports characteristic images of the TiO_2 atomic plume at two pressures representative of the regimes (a) and (b) of Fig. 1. In the left panels of Fig. 2(a) we observe that in HV the fast atomic plume is characterized by a very forward-peaked expansion into vacuum, reaching distances of few tens of mm from the target surface on a timescale of few hundred nanoseconds. At a delay of 2.5 μs, the atomic plume has significantly reduced its emission intensity and already moved to distances larger than ≈ 30 mm, and only the NPs plume, whose expansion only occurs after a much longer delay, is visible close to the target surface.

In the regime (b), the background gas pressure strongly affects the atomic plume expansion, as evidenced in the right panels of Fig. 2(a) corresponding to $p = 5 \times 10^{-2}$ mbar. From the images we can appreciate that in this regime the atomic plume expansion is effectively confined as its front follows an almost stationary behavior, while its shape becomes more spherical at longer delay. This indicates that the transition between regimes (a) and (b) is strictly related to the progressive confinement of the atomic plume, which is eventually halted over distances shorter than the

Atomic plume

(a)

HV 5×10^{-2} mbar

2.5 μs

0.25 μs

NPs plume

(b)

5×10^{-2} mbar   10 mbar

100 μs

10 μs
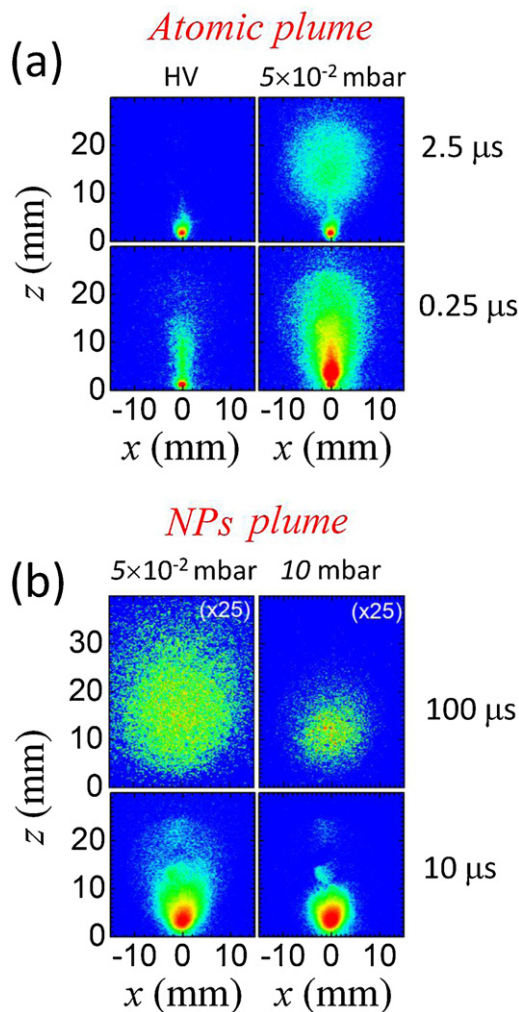
Fig. 2. Images of the TiO$_2$ plume emission at various delays τ (indicated on the right of the images) after the laser pulse. Panel (a) reports images of the atomic plume expansion in HV (left) and at $p = 5 \times 10^{-2}$ mbar (right), corresponding to the transition between the propagation regimes (a) and (b). The images were acquired at $\tau = 0.25$ μs and 2.5 μs with gate widths of 200 and 500 ns, respectively. Panel (b) shows images of the NPs plume expansion at $p = 5 \times 10^{-2}$ mbar (left) and $p = 10$ mbar (right), corresponding to the transition between the propagation regimes (b) and (c). The images were acquired at $\tau = 10$ μs and 100 μs, respectively, with a gate width of 5 μs. To facilitate the comparison, the intensity of the images of panel (a) was rescaled to the corresponding gate width, while the intensity of the images acquired at 100 μs in panel (b) was multiplied by an appropriate factor reported in parenthesis in the upper right corner. The plume propagation direction is along the z-axis, and $z = 0$ marks the position of the target surface, while the x-axis is parallel to the target surface. A logarithmic intensity scale is used to compensate for the differences in the emission intensities of the various components.

target-to-substrate distance for pressures larger than $\approx 10^{-2}$ mbar. As a consequence, the contribution of the atomic species to the amount of material deposited on the substrate is gradually reduced as the pressure increases, eventually becoming negligible in regime (b). The $\approx 30\%$ reduction of the deposition rate observed in Fig. 1 by passing from regime (a) to regime (b) also suggests a minor contribution of the atomic species to the overall amount of material ablated during ULA of TiO$_2$. This, in turn, demonstrates that also for semiconductor oxides ULA leads to a target decomposition which results in the prevalence of nanometer-size particulates, similarly to what was reported earlier for metals [18,36,37]. Fig. 2(b) reports characteristic images of the TiO$_2$ NPs plume at two pressures representative of the regimes (b) and (c) of Fig. 1. In the left panels of Fig. 2(b) we observe that in the regime (b) the NPs plume propagates into the background gas reaching distances comparable to

the target-to-substrate distance on a timescale of hundreds μs. Instead, at $p = 10$ mbar (Fig. 2(b), right panels), the NPs plume results significantly confined, and the NPs eventually stop before reaching the substrate, which explains the progressive reduction of the deposition rate observed in the regime (c).

Fig. 3 reports typical FESEM images of the TiO$_2$ NPs-assembled films. In the HV conditions, about 4×10^4 laser shots were used for film deposition. In the other two regimes, the number of laser pulses was rescaled according to the variation of the deposition rate shown in Fig. 1. In regimes (a) and (b), we observe the formation of a rather porous assembly of large globular nanostructures decorated with a number of smaller NPs (Fig. 3, upper left panel) with typical sizes of ≈ 10–20 nm. The film morphology resembles an agglomerated, colloidal-like nanostructure, with NPs embedded in a glue-like substance. On the contrary, regime (c) leads to a drastically different morphology of the deposited films (Fig. 3, upper right panel): an assembly of NPs, with typical sizes ranging from ≈ 20 to ≈ 200 nm, is produced, which is characterized by a highly porous nanostructure composed of individual NPs. This is also supported by the cross section images shown in the lower panels of Fig. 3. In regime (c) (Fig. 3, lower right panel), we observe that the NPs have a very spherical shape, creating a porous packed-ball system. Differently, in the cross section image of regimes (a) and (b), a number of rather shapeless and compact clusters is observed (Fig. 3, lower left panel).

A key difference between HV/intermediate pressures [regimes (a) and (b)] and high pressure [regime (c)] conditions is the change in the propagation dynamics of the ablated NPs. In the former case, the NPs expand in the background gas at high velocity, being eventually deposited along a line-of-sight trajectory, and impacting the substrate at high kinetic energy. On the contrary, in the latter case the NPs plume is halted over distances shorter than the target-to-substrate distance, and the NPs are eventually collected on the substrate after diffusion into the background atmosphere. This explains the noteworthy change of the film morphology, suggesting that appropriate tuning of the experimental parameters (e.g., background gas pressure, or target-to-substrate distance) can allow additional control on the morphology of the nanostructures produced by fs-PLD. Finally, Fig. 4 reports XRD patterns of the NPs-assembled films in the 2θ range 24.5–28.5°, where the most intense peaks of TiO$_2$ are expected, namely, A(101) for anatase (JPDS-84–1286), and R(110) for rutile (JPDS-88–1175). We observe that in regime (a)-(b) the as-grown films are composed of amorphous material, while in regime (c) the presence of a rutile peak indicates that crystalline NPs are mixed with amorphous ones. According to the Scherrer equation [21], the average size of these rutile nanocrystallites is ≈ 40–50 nm, comparable to the dimensions of the deposited NPs, which is shown in Fig. 3(c). The coexistence of amorphous and crystalline NPs in the material produced during ULA in background gas was reported earlier for silicon, and ascribed to the different cooling rates of the NPs depending on their size [19]. In particular, at high pressure the formation of a larger number of crystalline NPs was reported, similarly to what has been observed here for TiO$_2$ [19]. Instead, deposits formed by crystalline nanoclusters were obtained during fs-PLD of GaAs, with a thin amorphous oxide layer on the NPs forming upon air exposure [20]. The morphology of these GaAs deposits changed from a continuous solid film in high vacuum to a powder-like film at high Ar background pressure, which is consistent with our observations for TiO$_2$. This, in turn, indicates a peculiar role of the background gas pressure on the crystalline properties of the deposited TiO$_2$ nanostructures. In fact, our observations are also different from ns-PLD of TiO$_2$ where crystalline films are always obtained with the background gas pressure namely influencing the relative contributions of the anatase and rutile phases [29–31].
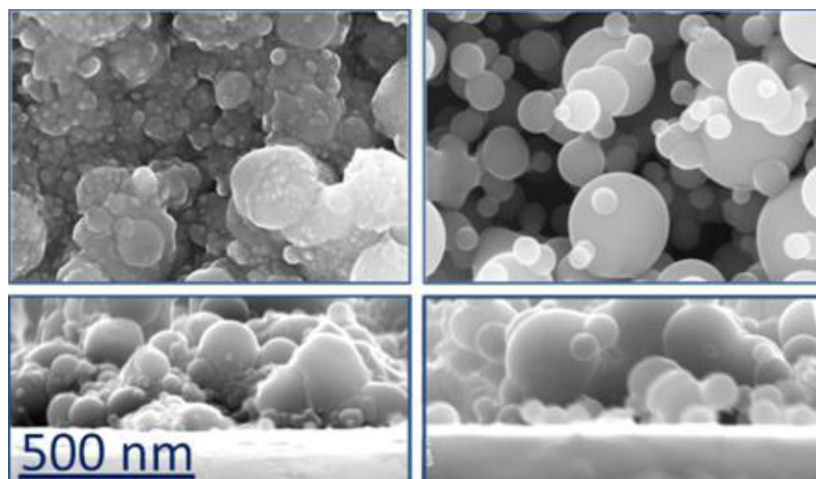
Fig. 3. Upper panels show representative FESEM images of TiO$_2$ NPs-assembled films. Left panel: regimes (a)–(b); right panel: regime (c). Lower panels report cross section images of TiO$_2$ NPs-assembled films. Left panel: regimes (a)–(b); right panel: regime (c).

In an attempt to improve the crystallinity of the NPs-assembled films, we carried out a preliminary analysis of the effects induced by a post-annealing treatment of the deposited samples. The NPs-assembled films were annealed in air for 30 min at 500 °C. Comparison of FESEM images, taken before and after annealing, indicates that no significant modification of both NPs-assembled film morphology and constituent NPs sizes occurs at such a temperature. On the other hand, the degree of crystallinity increases as indicated by the XRD patterns reported in Fig. 4. In particular, we observe that the annealing process favors crystallization, particularly for the anatase phase. In fact, annealing of the samples grown in regimes (a)–(b) results in the appearance of both anatase and rutile peaks, the anatase being slightly sharper than the rutile one. For regime (c), while the rutile peak does not change significantly with respect to the as-grown sample after the annealing process, the anatase peak is also observed. According to Scherrer equation [21], crystallites formed in the samples deposited in regimes (a)–(b) have, after annealing, average sizes of ≈20 nm for R(1 1 0) and ≈40 nm for A(101). For the samples grown in the regime (c), the R(1 1 0) crystallites sample are ≈40–50 nm for both the as-grown and annealed samples, while the A(1 0 1) crystallites formed through annealing are ≈70 nm, respectively. This seems to suggest that for the sample morphology of regimes (a)–(b), the crystallization actually involves only the small NPs decorating the larger aggregated nanostructures, while for regime (c) it affects more generally the individual building blocks of the NPs-assembled film. This also evidences that the annealing treatment only results in an improved structural ordering of the particles, while particle size growth and/or coalescence is likely hindered by the open morphology.

4. Conclusions

In conclusion, we have investigated the effects of the background oxygen pressure on the properties of TiO$_2$ NPs-assembled films produced by fs-PLD. The film morphology changes from a cauliflower-like structure, with NPs embedded in glue-like nanoagglomerates, at low pressure (<1 mbar), to a highly porous assembly of individual NPs, at larger pressure (>1 mbar). ICCD imaging and deposition rate measurements allowed correlating these observations with the presence of different regimes in the propagation dynamics of the atomic and NPs plumes produced by ULA of TiO$_2$. At low pressure, the produced NPs impact on the substrate at higher velocity, which favors the formation of agglomerated structures. On the contrary, the effective confining effect of the background gas achieved at pressures of few mbar leads to a diffusive propagation of the NPs towards the substrate. This, in turn, results in a porous assembly of individual NPs. The as-grown nanostructures are composed of amorphous material, but preliminary post-annealing experiments allow anticipating the possibility of modifying their crystalline state by appropriate thermal treatment. Our experimental findings demonstrate an interesting influence of the background gas pressure on the properties of the TiO$_2$ NPs-assembled films, which is of general interest. These results confirm the interesting possibility of tuning oxide NPs-assembled films structural characteristics by appropriate selection of the deposition conditions offered by ns-PLD and fs-PLD, also evidencing some interesting differences for the case of a semiconductor oxides like TiO$_2$. For instance, amorphous TiO$_2$ nanostructures are produced at lower background pressure with the formation of a minor rutile crystalline component at larger pressure. Comparison with previous result of ULA of semiconductors, in a background gas and at room temperature, show coherence with the case of silicon [19], but interesting differences are observed with respect to GaAs, where crystalline NPs are always observed [20]. This evidences some peculiarities of the TiO$_2$ fs-PLD which deserve further investigation for other semiconductor oxides.

Finally, the porosity at the nanoscale, as well as the high surface-to-volume ratio brought about by the oxide NPs assembly produced
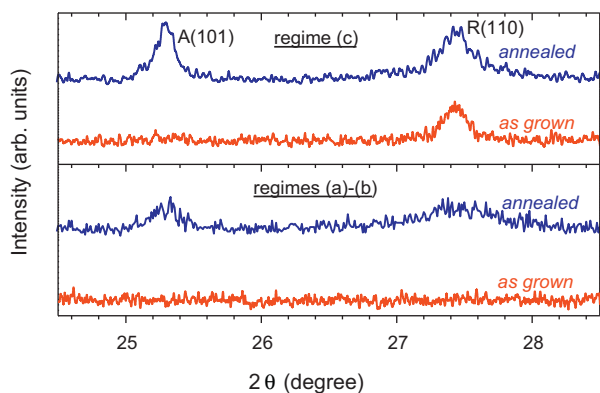
Fig. 4. XRD patterns of TiO$_2$ NPs-assembled films. Bottom panel: regimes(a)–(b); Upper panel: regime (c). The red curves refer to as-grown films, while the blue curves correspond to the XRD pattern after the annealing treatment.

by fs-PLD in a background gas, can be helpful in fabricating oxide nanostructures facilitating reactions with the interacting medium in photocatalytic, and sensing applications.

Acknowledgements

References

[1] O. Albert, S. Roger, Y. Glinec, J.C. Loulergue, J. Etchepare, C. Boulmer-Leborgne, J. Perrière, E. Million, Applied Physics A 76 (2003) 319.
[2] S. Amoruso, R. Bruzzese, N. Spinelli, R. Velotta, M. Vitiello, X. Wang, G. Ausanio, V. Iannotti, L. Lanotte, Applied Physics Letters 84 (2004) 4502.
[3] S. Eliezer, N. Eliaz, E. Grossman, D. Fisher, I. Gouzman, Z. Henis, S. Pecker, Y. Horovitz, M. Fraenkel, S. Maman, Y. Lereah, Physical Review B 69 (2004) 144119.
[4] S. Amoruso, G. Ausanio, R. Bruzzese, M. Vitiello, X. Wang, Physical Review B 71 (2005) 033406.
[5] G. Ausanio, A.C. Barone, V. Iannotti, L. Lanotte, S. Amoruso, R. Bruzzese, M. Vitiello, Applied Physics Letters 85 (2004) 4103.
[6] M. Sanz, R. de Nalda, J.F. Marco, J.G. Izquierdo, L. Bañares, M. Castillejo, Journal of Physical Chemistry C 114 (2010) 4864.
[7] A. Oguz Er, W. Ren, H.E. Elsayed-Ali, Applied Physics Letters 98 (2011) 013108.
[8] E. Millon, J.C. Loulergue, J. Etchepare, D. Hulin, W. Seiler, J. Perrière, Journal of Applied Physics 88 (2000) 6937.
[9] E. Millon, J. Perrière, R.M. Défourneau, D. Défourneau, O. Albert, J. Etchepare, Applied Physics A 77 (2003) 73.
[10] M. Sanz, M. Walczak, R. de Nalda, M. Oujja, J.F. Marco, J. Rodriguez, J.G. Izquierdo, L. Bañares, M. Castillejo, Applied Surface Science 255 (2009) 5206.
[11] B. Liu, Z. Hu, Y. Che, Y. Allenic, K. Sun, X. Pan, Applied Physics A 93 (2008) 813.
[12] Y. Zhang, R.E. Russo, S.S. Mao, Applied Physics Letters 87 (2005) 133115.
[13] R. Eason (Ed.), Pulsed Laser Deposition of Thin Films: Applications-led Growth of Functional Materials, Wiley, Hoboken, NJ, 2006.
[14] D.B. Chrisey, G.K. Hubler (Eds.), Pulsed Laser Deposition of Thin Films, Wiley, New York, 2004.
[15] A. Sambri, S. Amoruso, X. Wang, M. Radovic', F. Miletto Granozio, R. Bruzzese, Applied Physics Letters 91 (2007) 151501.
[16] S.S. Harilal, C.V. Bindhu, M.S. Tillack, F. Najmabadi, A.C. Gaeris, Journal of Applied Physics 93 (2003) 2380.
[17] S. Amoruso, B. Toftmann, J. Schou, Physical Review E 69 (2004) 056403.
[18] S. Amoruso, R. Bruzzese, X. Wang, J. Xia, Applied Physics Letters 92 (2008) 041503.
[19] B.R. Tull, J.E. Carey, M.A. Sheehy, C. Friend, E. Mazur, Applied Physics A 83 (2006) 341.
[20] L.N. Dinh, S.E. Hayes, A.E. Wynne, M.A. Wall, C.K. Saw, B.C. Stuart, M. Balooch, A.K. Paravastu, J.A. Reimer, Journal of Materials Science 37 (2002) 3953.
[21] X. Chen, S.S. Mao, Chemical Reviews 107 (2007) 2891.
[22] F. Di Fonzo, C.S. Casari, V. Russo, M.F. Brunella, A. Li Bassi, C.E. Bottani, Nanotechnology 20 (2009) 015604.
[23] V. Zorba, X. Chen, S.S. Mao, Applied Physics Letters 96 (2010) 093702.
[24] R. Ciancio, E. Carlino, C. Aruta, D. Maccariello, F. Miletto Granozio, U. Scotti di Uccio, Nanoscale 4 (2012) 91.
[25] M. Batzill, U. Diebold, Progress in Surface Science 79 (2005) 47.
[26] S. Lettieri, A. Bismuto, P. Maddalena, C. Baratto, E. Comini, G. Faglia, G. Sberveglieri, L. Zanotti, Journal of Non-Crystalline Solids 352 (2006) 1457.
[27] C. Baratto, S. Todros, G. Faglia, E. Comini, G. Sberveglieri, S. Lettieri, L. Santamaria, P. Maddalena, Sensors and Actuators B: Chemical 140 (2009) 461.
[28] A. Fujishima, T.N. Rao, D.A. Tryk, Journal of Photochemistry and Photobiology C 1 (2000) 1.
[29] T. Nambara, K. Yoshida, L. Miao, S. Tanemura, N. Tanaka, Thin Solid Films 515 (2007) 3096.
[30] M. Walczak, M. Oujja, J.F. Marco, M. Sanz, M. Castillejo, Applied Physics A 93 (2008) 735.
[31] M. Sanz, M. Walczak, M. Oujja, A. Cuesta, M. Castillejo, Thin Solid Films 517 (2009) 6546.
[32] E. Gÿorgy, A. Pérez del Pino, G. Sauthier, A. Figueras, F. Alsina, J. Pascual, Journal of Physics D: Applied Physics 40 (2007) 5246.
[33] J.M. Liu, Optics Letters 7 (1982) 196.
[34] J. Bonse, S. Baudach, J. Krüger, W. Kautek, M. Lenzner, Applied Physics A 74 (2002) 19.
[35] M. Sanz, M. Castillejo, S. Amoruso, G. Ausanio, R. Bruzzese, X. Wang, Applied Physics A 101 (2010) 639.
[36] M.E. Povarnitsyn, T.E. Itina, M. Sentis, K.V. Khishchenko, P.R. Levashov, Physical Review B 75 (2007) 235414.
[37] S. Amoruso, R. Bruzzese, X. Wang, N.N. Nedialkov, P.A. Atanasov, Journal of Physics D 40 (2007) 331.